Encapsulation and Enzyme-Mediated Release of Molecular Cargo in Polysulfide Nanoparticles

Brett L. Allen,* Jermaine D. Johnson, and Jeremy P. Walker

FLIR Systems, Inc., 2240 William Pitt Way, Pittsburgh, Pennsylvania 15238, United States

ABSTRACT Poly(propylene sulfide) nanoparticles (<150 nm) have been synthesized by an anionic, ring-opening emulsion polymerization. Upon exposure to parts per million (ppm) levels of oxidizing agent (NaOCl), hydrophobic polysulfide particles are oxidized to hydrophilic polysulfoxides and polysulfones. Utilizing this mechanism, the encapsulation of hydrophobic molecular cargo, including Nile red and Reichardt's dye, within polysulfide nanoparticles has been characterized by a variety of microscopic and spectroscopic methods and its release demonstrated *via* chemical oxidation. Moreover, release of cargo has been enzymatically driven by oxidoreductase enzymes such as chloroperoxidase and myeloperoxidase in the presence of low concentrations of sodium chloride (200 mM) and hydrogen peroxide (500 μM). This oxidation-driven mechanism holds promise for controlled encapsulation and release of a variety of hydrophobic cargos.

KEYWORDS: nanoparticles · emulsion polymerization · polysulfide · enzyme catalysis · cargo · controlled release

Nanostructured particle systems have recently been developed for applications in medical diagnostics and therapy.[1−3] Such systems are typically of the hollow nano- or microcapsule variety, generally a colloidal drug carrying system composed of an organic or aqueous core surrounded by a polymer shell.[4,5] Some nanocapsules, based on layer-by-layer adsorption of oppositely charged macromolecules to a colloidal template, have been found to encapsulate species such as fluorescent quantum dots[6] and magnetic nanoparticles.[7] Moreover, it has been observed that particle permeability may be altered through pH-responsive interactions, alluding to quasi-controlled external stimuli facilitating loading and/or release of encapsulated cargo.[8] For instance, researchers have demonstrated the formation of acid-degradable microcapsules prepared *via* interfacial polymerization.[9] These microparticles not only have delivered and released cargo into cells but also showed that upon degradation, byproducts consisted of acetone and a nontoxic triamide. Further, an increase in polymeric nanoparticle systems based on poly(lactic acid),[10] poly(alkyl cyanoacrylates),[11] or biodegradable chitosan has been observed.[12,13] While effective in their sustained release of encapsulated cargo (*e.g.*, drugs) through hydrolysis-induced degradation, polymeric nanoparticles are not necessarily responsive to specific external stimuli generated from a potential physiological response.

Of particular interest is the ability to generate a triggered nanoparticle response (*e.g.*, release of cargo) in the presence of oxidizing conditions. Cellular inflammation, a highly oxidative environment, is part of the nonspecific immune reaction that occurs as a response to harmful stimuli such as pathogens, foreign bodies, and damaged cells, resulting in their neutralization.[14] Triggered by cellular stress, oxidative conditions could also serve to stimulate the release of encapsulated drugs used to treat infection. Thus, some groups have attempted to utilize oxidative conditions for cargo release in a variety of ways. Water-soluble dextran particles have been shown to degrade and release cargo in response to 1 mM H_2O_2.[15] Similarly, oxidation-responsive polymeric micelles based upon poly(ethylene glycol)-*b*-acrylic acid and selenium-containing surfactant have been shown to degrade in the presence of 0.1% H_2O_2.[16] Of particular note, poly(propylene sulfide) (PPS), a hydrophobic polymer, is readily oxidized to form hydrophilic poly(sulfoxide) and poly(sulfone) in the presence of mild oxidizing agents. Utilizing this matrix for the encapsulation of hydrophobic drugs, natural oxidative responses such as inflammation could be used as a trigger for cargo release. In pursuit of this endeavor, groups have synthesized PPS nanoparticles through an anionic emulsion polymerization technique.[17,18] Upon exposure to mild oxidizing agents, thioesters, disulfides, and residual thiols of PPS nanoparticles are oxidized to hydrophilic sulfoxides and sulfones, resulting in the swelling

* Address correspondence to brett.allen@flir.com.

Received for review April 21, 2011 and accepted May 19, 2011.

Published online May 19, 2011
10.1021/nn201477y

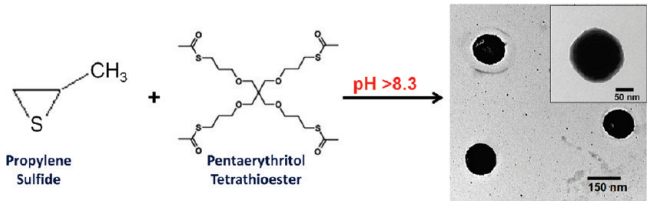

Figure 1. The anionic emulsion polymerization of PPS particles proceeds by the addition of propylene sulfide and activated pentaerythritol tetrathioester and initiation under basic conditions. Discrete PPS nanoparticles are formed with diameters of approximately 120 nm, as shown by transmission electron microscopy.

of nanoparticles. These particles have shown a vast degree of utility. Rehor *et al*. were able to selectively label PPS nanoparticles with reporter molecules (such as gold or fluorophores) and examine their uptake by microphages *in vitro* and blood circulation *in vivo*.[19] Factors such as surface composition and particle size were investigated to ascertain their influence on uptake. Furthermore, researchers have extended such progress to specific targeted tissues. Rothenfluh *et al*. demonstrated matrix binding to articular cartilage, specifically the cartilage matrix component collagen II α1, by modifying PPS nanoparticles (38 nm diameter) with high-affinity peptides.[20] Targeted nanoparticles immobilized within the cartilage matrix were shown to persist for 96 h without significant clearance. While significant progress has been made, interior encapsulation and enzymatic release of cargo has yet to be demonstrated.

In this work, we synthesize PPS nanoparticles by anionic emulsion polymerization. The addition of hydrophobic cargo such as solvatochromic dyes such as Reichardt's dye or fluorescent dyes such as Nile red dye during the polymerization process results in their stabilization in aqueous media through encapsulation. The addition of mild oxidizing agents, *e.g*., low, localized levels of sodium hypochlorite (NaOCl), causes particle oxidation, subsequent swelling, and release of molecular cargo. Moreover, we demonstrate this oxidative release can be facilitated through peroxidase enzyme oxidant generation. Chloroperoxidase (CPO) and human myeloperoxidase (hMPO) (both heme-containing oxidoreductase enzymes), in the presence of 200 mM NaCl and 500 μM H_2O_2, generate hypochlorous acid (HOCl), which oxidizes PPS nanoparticles and causes the release of encapsulated molecular cargo.

RESULTS AND DISCUSSION

Poly(propylene sulfide) nanoparticles were synthesized using a modified anionic polymerization methodology based upon previous work.[17] Approximately 1% w/v of Pluronic F-127 surfactant was added to deionized (DI) water and then degassed under N_2. Propylene sulfide, an episulfide, was then added to the reactor followed by activated pentaerythritol tetrathioester. To initiate the anionic "ring-opening" emulsion polymerization, the system pH is generally increased above 8.3 (pK_a for thiol) to deprotonate free thiols. Most commonly, diaza[5.4.0]bicycloundec-7-ene (DBU) is added as a basic initiator. We found, however, that the addition of 10% borate buffer (100 mM, pH 9.0) was sufficient to initiate the reaction. The polymerization then proceeded for 24 h, before capping free reactive thiol groups by iodoacetamide (IDA) or allowing disulfide linkages to occur through air oxidation. Figure 1 illustrates the emulsion polymerization with resultant transmission electron microscopy (TEM) characterization.

Synthesized PPS nanoparticles were cleaned from unreacted monomer by dialyzing against DI water for two weeks with daily changes of dialysate. A single drop of colloidal particles suspended in DI water was then placed on a carbon-coated TEM grid and imaged using an 80 keV Morgagni FEI TEM. As observed by microscopic analysis, PPS nanoparticles are approximately 120 $\pm$ 40 nm in diameter (internal volume average: 2.99 $\times$ 10^{-16} cm^3, Supporting Information) based upon 50 point-to-point measurements. Furthermore, dynamic light scattering data confirm this particle size distribution with a polydispersity index of 0.31 (Supporting Information). These hydrophobic PPS nanoparticles retained their stability in aqueous environments for >6 months owing to the Pluronic surfactant layer entangled within the PPS polymer matrix. Of important note, however, the addition of oxidizing agents to a suspension of colloidal PPS nanoparticles should cause the hydrophobic polysulfide matrix to oxidize to polysulfoxides and polysulfones, resulting in increased hydrophilicity and particle swelling (Figure 2A). Such swelling can be tracked on a UV−vis spectrophotometer by turbidity measurements that monitor visible light scattering at 600 nm.

To test this unique characteristic of PPS nanoparticles, we examined particle oxidation with sodium hypochlorite (NaOCl) at pH 6.02 to promote optimal formation of hypochlorous acid.[21] Briefly, a 10 mL aliquot of PPS particles suspended in DI water was centrifuged at 8000 rpm for 10 min. The supernatant was discarded, and the pellet was resuspended in an equal volume of 100 mM phosphate buffer (pH 6.02) through mild agitation. Approximately 200 μL of PPS aliquots in buffer were further diluted to 2 mL and tested against various concentrations of NaOCl ranging from 25 ppm (ppm) to 200 ppm, added as 10 μL

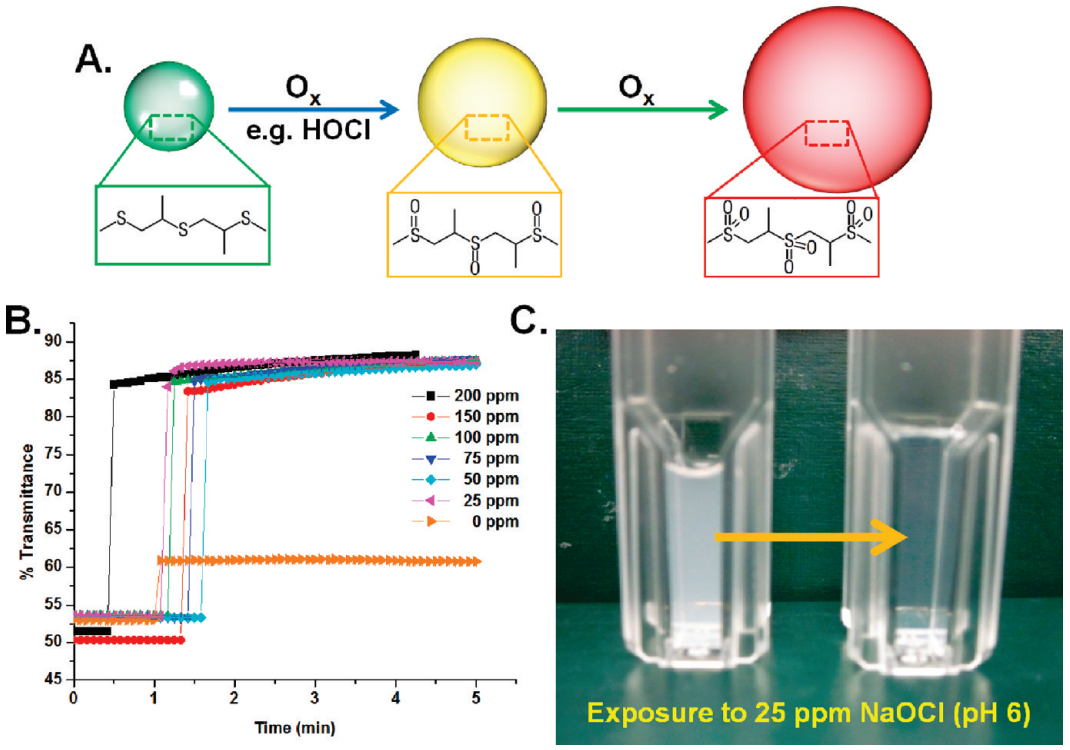

Figure 2. (A) Schematic representation of progressive oxidation of sulfides, resulting in sulfoxide and sulfone formation with increased particle swelling. (B) Particle turbidity (% transmittance) monitored at 600 nm demonstrates an immediate response to oxidizing NaOCl at concentrations as low as 25 ppm. (C) Photograph illustrating visual changes in particle turbidity in response to 25 ppm of NaOCl.

volumes. A 10 μL addition of buffer (0 ppm) shows the effect of dilution. Shown in Figure 2B, PPS particle turbidity at 600 nm was monitored over time before and after the addition of NaOCl.

Transmittance measurements were taken as a function of time to ascertain the effect of oxidizing agent presence. A stable baseline was observed for approximately 30 s to 1 min prior to the addition of varying concentrations of NaOCl. As demonstrated, concentrations of NaOCl, added as low as 25 ppm (10 μL), resulted in an immediate increase in transmittance from ~50% to 90%. Moreover, it was observed that such an increase in transmittance was not due to sample dilution, as an equal volume of buffer added to the system elicited a change of only 10%. This change could also be visually confirmed as shown in Figure 2C. The turbid sample, upon exposure to 25 ppm, undergoes an immediate change toward increasing transparency. Such transparency is analogous to that previously reported,[22] where conversion of hydrophobic polysulfides to soluble, nonscattering polysulfones was observed. The decrease in scattering light intensity presumably occurs, as the n_{av} (average refractive index) of oxidized PPS nanoparticles ($n_{av} = n_{PPS}\Phi_{PPS} + n_{H2O}\Phi_{H2O}$) more closely resembles that of the surrounding aqueous media.

This colloidal system may potentially have utility as cargo-carrying vessels, susceptible to stimuli-responsive (oxidative) release. To progress with this hypothesis, slight modification of the PPS nanoparticle synthesis procedure was performed. Specifically, after the addition of 1% surfactant, a hydrophobic dye was added to the system and allowed to solubilize in the reactor prior to the addition of propylene sulfide and activated pentaerythritol tetrathioester. Hydrophobic Reichardt's dye[23] (a solvatochromic dye) was thus added to the reactor at a concentration of 0.01% w/v. Following the 24 h reaction, Reichardt's dye was solubilized in aqueous media as illustrated in Figure 3A. The initial colloidal suspension (prior to centrifugation) was characterized using solid-state reflectance spectroscopy, which yielded a prominent peak at 440 nm. Upon centrifugation of a 2 mL aliquot at 8000 rpm for 10 min, a blue pellet was observed that could be resuspended in DI water, alluding to encapsulation within PPS nanoparticles. To test the potential for oxidative release of Reichardt's dye in PPS particles, a centrifuged pellet was resuspended in an equal volume of 100 mM phosphate buffer at pH 6.02. In addition to removing free monomer associated with the polymerization, residual IDA is also removed from the system, which may precipitate as I_2 in the presence of oxidizing agent. As indicated in Figure 3A, reflectance measurements demonstrate ~40% loss in intensity at 440 nm, presumably a result of the purification process removing smaller PPS particles and residual monomer. This sample was then subjected to oxidation by 2000 ppm NaOCl and allowed to equilibrate for 5 min prior to additional reflectance

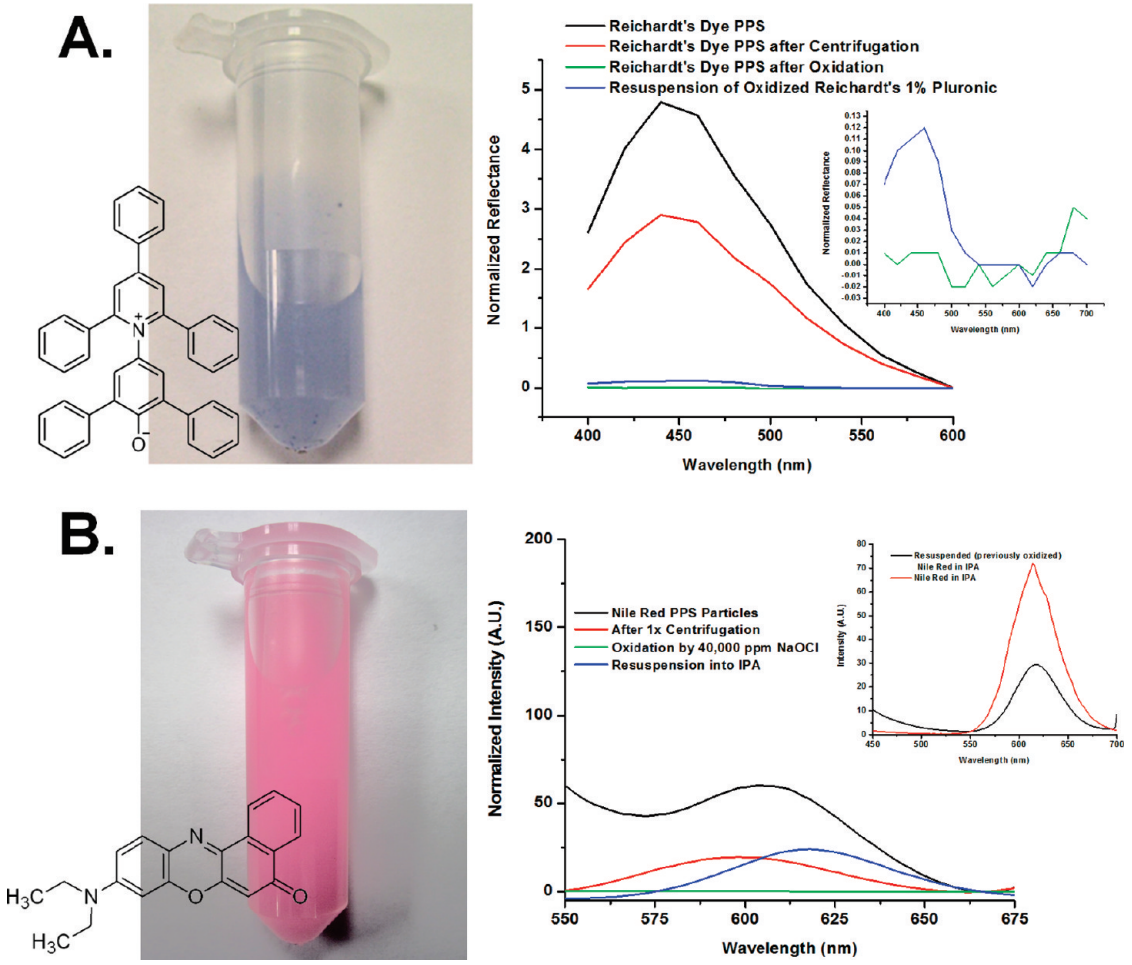

Figure 3. (A) Encapsulation of Reichardt's dye yields a soluble, blue colloidal suspension. Reflectance measurements track encapsulation, oxidative release with 2000 ppm NaOCl addition, and recovery by centrifugation and resuspension in 1% w/v Pluronic (inset). (B) Analogous hydrophobic Nile red dye is encapsulated using the same approach. Spectrofluorimetric measurements monitor oxidative release and recovery by resuspension into isopropyl alcohol (IPA) (inset).

measurements. Upon oxidation and characterization by reflectance spectroscopy, a 98% reduction in signal intensity at 440 nm was observed, alluding to the destabilization of Reichardt's dye in PPS nanoparticles. In an attempt to recover precipitated dye, centrifugation was performed at 18 000 rpm for 5 h. The supernatant was then discarded, and small blue flakes were resuspended in 2 mL of 1% w/v Pluronic F127. Reflectance measurements indicate that ~4% of the original intensity from Reichardt's dye could be recovered through stabilization in surfactant. Such a low yield of recovery indicates that some dye may be lost in the supernatant during centrifugation, or limited solubility prevents its resuspension in 1% surfactant. Indeed, whenever dye was resuspended in acetone (in lieu of 1% surfactant), almost 100% recovery was observed according to reflectance measurements (Supporting Information). To confirm that dye oxidation was not responsible for signal loss, a control of 100 mM Reichardt's dye in 1% Pluronic was also exposed to 2000 ppm NaOCl. No noticeable decrease in intensity was observed as a result of exposure (Supporting Information).

As an extension of this study, we sought to encapsulate other hydrophobic species and to demonstrate the utility of this approach. Identical to work performed for the encapsulation of Reichardt's dye, Nile red dye was added to a polymerization reaction at <0.01% w/v. Prepared from Nile blue, Nile red is an intensely fluorescent, hydrophobic dye commonly utilized in the staining of intracellular lipids.[24] Depending upon the solvent hydrophobicity, the excitation and emission maxima of Nile red fluorescence can vary over a range of 60 nm.[25] Following the 24 h reaction, Nile red appeared to be stabilized in aqueous media by the assistance of PPS nanoparticles (Figure 3B). Particles remained suspended for up to 6 months and stable in the presence of excess surfactant (Pluronic F-127). A spectrofluorimetric examination (λ_{ex}: 485 nm) of the raw reaction contents demonstrated an intense emission peak at ~600 nm. Taking into consideration the amount of Nile red added to the system, 3.1% efficiency of encapsulation was observed based upon liquid–liquid extraction into hexane (Supporting Information). To validate oxidative release of Nile red

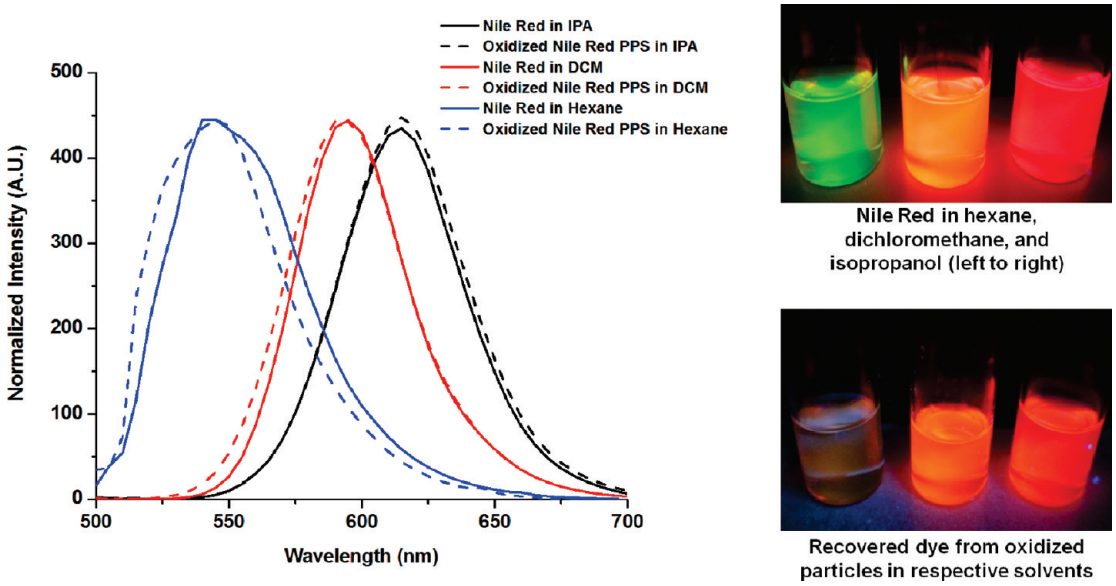

Figure 4. Nile red dye initially solubilized in hexane, dichloromethane, and isopropyl alcohol exhibited characteristic emission based upon solvent polarity. After recovering encapsulated Nile red released through chemical oxidation and resuspending in each solvent, no emission shifts indicative of dye oxidation were observed.

dye encapsulated within PPS particles, a 2 mL aliquot was centrifuged at 8000 rpm for 10 min. The pink pellet was resuspended in an equal volume of 100 mM phosphate buffer (pH 6.02). Following resuspension through gentle agitation and spectrofluorimetric characterization, approximately 67% of the initial emission intensity was lost presumably due to particle losses during centrifugation purification. This sample was then exposed to 2000 ppm NaOCl and left to incubate for 5 min (Supporting Information). Upon examining the sample, we observed a complete loss of spectroscopic features. Such a loss may be present as a result of precipitation of the hydrophobic dye from PPS particles or dye oxidation resulting in fluorescence quenching. To elucidate if precipitation was responsible for the "quenching" effect, the oxidized aliquot was centrifuged at 18 000 rpm for 5 h. Since PPS nanoparticles are completely oxidized and hydrophilic, they remained in the discarded supernatant. The small dye pellet was then resuspended in isopropyl alcohol (IPA), as attempts to solubilize Nile red in 1% surfactant were unsuccessful. As illustrated in Figure 3B, emission intensity is recovered, albeit red-shifted 20 nm from the original emission peak. This emission was then compared to Nile red dye solubilized in IPA (no oxidation). Expectedly, the change in solvent polarity was found to be responsible for the emission peak shift, as indicated by the inset.

Further controls were performed to verify Nile red encapsulation and resistance to dye oxidation. PPS nanoparticles were synthesized as previously described, without the addition of a hydrophobic cargo. After centrifuging at 8000 rpm for 5 min and resuspending the resultant pellet in 2 mL of 100 mM phosphate buffer (pH 6.02), 0.02% w/v of Nile red dye was added to the aliquot and left to incubate for 24 h. Hydrophobic Nile red should be unable to partition into particles or adsorb to the surface because of the Pluronic surfactant shell stabilizing PPS nanoparticles. Indeed, after 24 h the dye was still precipitated in the presence of solubilized PPS particles. Spectrofluorimetric analysis (Supporting Information) exhibited no notable spectroscopic features that would be indicative of Nile red stabilization. Furthermore, in-depth oxidation studies were performed to ascertain any degree of Nile red oxidation during its release in PPS particles. Nile red is capable of solubilizing in a wide range of organic solvents such as toluene, cyclohexane, and dimethylformamide. We have exploited this solubility by examining Nile red in hexane, dichloromethane (DCM), and IPA and comparing emission profiles to that obtained by encapsulated Nile red released by 2000 ppm NaOCl and resuspended in one of these respective solvents. To ascertain the appropriate excitation wavelength for Nile red in hexane, DCM, or IPA, respectively, spectral mapping was performed by exciting from 400 to 490 nm and monitoring emission from 500 to 700 nm (Supporting Information). On the basis of the obtained three-dimensional plots, it was found that Nile red could be excited at 480 nm in IPA and DCM and at 440 nm in hexane without appreciable overlap in fluorescent emission. Figure 4 illustrates the initial differences in Nile red emission in each solvent. As can be seen, Nile red demonstrates a polarity-based emission peak at 545 nm (green) in hexane, at 595 nm (orange) in DCM, and at 615 nm (red) in IPA. In comparison, when encapsulated Nile red was recovered from an oxidized PPS system (through centrifugation) and resuspended in each of these respective solvents, no noticeable emission peak was observed. It has been previously

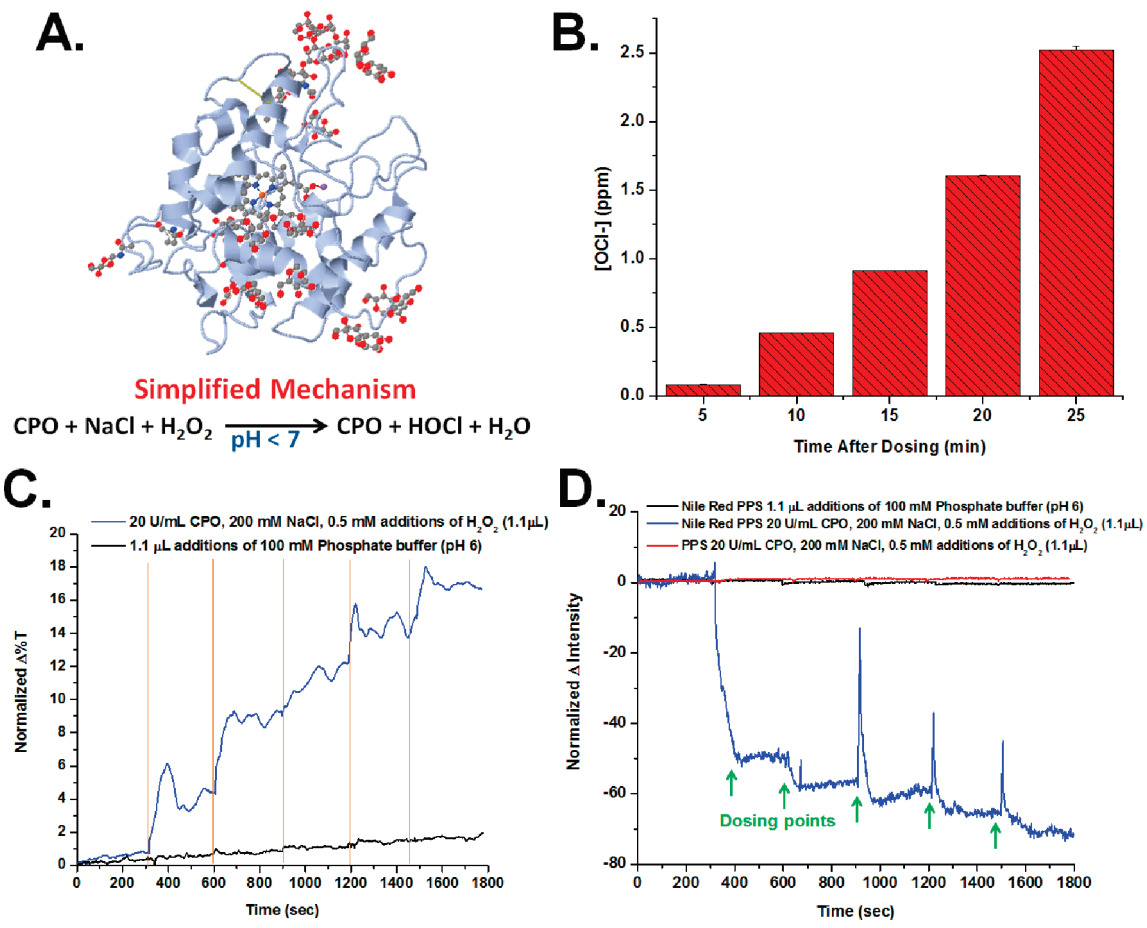

Figure 5. (A) Tertiary structure of chloroperoxidase and its catalytic conversion of NaCl and H_2O_2 to HOCl. (B) Generated ROS/HOCl as 20 U/mL CPO is dosed with 500 μM H_2O_2 every 5 min. (C) Normalized turbidity measurements of PPS particle swelling induced by CPO ROS generation. (D) Normalized spectrofluorimetric measurements of Nile red release by CPO-mediated PPS particle swelling. Spikes indicate detector saturation upon dosing.

reported that Nile red, when oxidized, exhibits a blue-shift in its absorbance and emission spectra.[26] However, these data demonstrate no such shift in emission spectra after the presence of an oxidizing agent. Thus, observed quenching of Nile red encapsulated by PPS nanoparticles in the presence of 2000 ppm NaOCl must be the result of its release and poor water solubility,[24] leading to precipitation.

While chemical oxidation by NaOCl demonstrated an active "trigger" for PPS nanoparticle swelling and subsequent release of molecular cargo including hydrophobic Reichardt's and Nile red dyes, it is highly advantageous to elicit analogous responses through biologically active species. For instance, enzymes (specifically oxidoreductase enzymes) have demonstrated the ability to oxidize a wide variety of substrates such as small molecules[27] and even inert carbon nanotubes.[28,29] Peroxidase enzymes including those of chloroperoxidase, horseradish peroxidase, and human myeloperoxidase have demonstrated the ability to generate a wide range of reactive oxygen species.[30] Thus, careful selection of a peroxidase enzyme should enable the oxidation of PPS nanoparticles and elicit release of molecular cargo in the presence of proper (noncompetitive) substrates.

To maintain an analogous comparison between chemical oxidation by NaOCl and potential oxidation by a biological species, we chose to work with chloroperoxidase to elicit particle swelling. Chloroperoxidase (EC 1.11.1.10, pH optimum: 2.75) is known to generate a variety of reactive oxygen species (ROS) depending upon the chemical substrates turned over by the enzyme. Generally, CPO has been utilized to generate chlorine dioxide (ClO_2) from sodium chlorite ($NaClO_2$);[31] however, in the presence of NaCl and H_2O_2 (at acidic pH) HOCl is generated (Figure 5A).[32,33] Since HOCl is the desired oxidant in these studies, we have employed CPO to produce a potential oxidative response in PPS particles through the addition of NaCl and H_2O_2 substrates. As a primary control, PPS particles were examined in the presence of varying concentrations of H_2O_2 (a known oxidant) in the range of 500 μM to 3 mM (Supporting Information). While the oxidation strength of H_2O_2 (1.78 V) is greater than that of HOCl (1.49 V), the kinetics for H_2O_2 oxidation are extremely slow.[34] Thus, we examined oxidation of PPS particles by

H_2O_2 within a 30 min time regime. As observed in the Supporting Information, no significant change in particle turbidity (relative to dilution) was present, indicating that any potential change in turbidity in the presence of enzyme is not because of oxidation by H_2O_2.

CPO was next optimized for its ability to produce relevant ROS by altering the concentration of NaCl and H_2O_2 relative to a fixed concentration of CPO (Supporting Information). For these studies, CPO concentration was fixed at a concentration of 20 U/mL. Chlorinated ROS were evaluated using an assay with *N*,*N*-diethyl-*p*-phenylenediamine (DPD) sulfate as an indicator.[35] DPD, when oxidized, generates a characteristic absorbance at 540 nm linearly proportional to oxidant concentration. A calibration plot was generated from a stock bottle of NaOCl, assessing concentrations from 250 ppb to 5 ppm (Supporting Information). At 20 U/mL of CPO, we found that NaCl concentrations between 200 and 300 mM and an H_2O_2 concentration of 500 μM, dosed every five minutes (Figure 5B), generated up to 3 ppm of ROS over 30 min without significantly diminishing enzyme activity. Of important note, while CPO's optimum activity is observed at pH 2.75, we have performed studies at pH 6.02 to keep consistency throughout the experiments.

While complete particle oxidation has been demonstrated in the presence of 2000 ppm NaOCl, it was uncertain to what extent 3 ppm of ROS causes particles to swell, or whether minor swelling was significant enough to result in the release of molecular cargo. To test the potential of CPO to elicit PPS particle swelling, 20 U/mL CPO (100 mM phosphate buffer pH 6.02) was added to an aliquot of particles with 200 mM NaCl. Every five minutes 500 μM H_2O_2 was added to the particles and the turbidity change observed. As illustrated in Figure 5C, a stable baseline was obtained for PPS particles for the first 300 s of turbidity measurements (600 nm). Slight drift was observed, presumably as a result of larger particle sedimentation, as this was noticed in all samples tested. Upon the first dose of 500 μM H_2O_2, the transmittance was observed to increase approximately 4% relative to the initial baseline. Further, each subsequent dose elicited a relative transmittance increase of ~3.5%. This appears to be in direct agreement with results pertaining to the assessment of ROS by dosing CPO (Figure 5B). As a comparison, PPS particles were also subjected to five equal-volume doses of 100 mM phosphate buffer (pH 6.02). Shown as the black trace in Figure 5C, it is quite evident that the addition of buffer (1.13 μL) to the 2 mL aliquot volume did not alter the transmittance of particles over the same 30 min time frame. Thus, the overall 18% change in transmittance was a result of particle oxidation by CPO-generated ROS.

Further spectrofluorimetric studies were performed to ascertain whether this degree of swelling was sufficient to promote the release of molecular cargo (Nile red dye). Utilizing the same conditions as performed for turbidity measurements, an aliquot of PPS-encapsulated Nile red particles was subjected to 20 U/mL CPO in the presence of 200 mM NaCl and dosed with 500 μM H_2O_2 every five minutes. A stable baseline was once again recorded during the first five minutes of testing, prior to the addition of 1.13 μL of H_2O_2. Upon the first dose, a 50% decrease in emission intensity (λ_{ex}: 485 nm, λ_{em}: 600 nm) relative to the five-minute baseline was observed, as indicated in Figure 5D and corresponding to the 4% increase in turbidity as previously observed. Each subsequent dose appears to generate an additional 5−10% decrease in emission intensity. Such trends suggest that most of the dye precipitated from the initial dose, followed by residual precipitation upon subsequent doses. To confirm that particle swelling was not a factor causing apparent emission intensity decrease, a control was performed with PPS particles lacking any encapsulated cargo. Shown as the red trace in Figure 5D, no observable decrease in emission intensity was present. Furthermore, dosing PPS-encapsulated Nile red particles with buffer demonstrated no significant dilution effects. Such data support the enzymatic oxidation of PPS particles and resultant release of Nile red dye into the aqueous environment leading toward emission quenching.

As a further extension of this work and confirmation of enzyme-mediated oxidation, a second oxidoreductase enzyme was utilized. Human myeloperoxidase (EC 1.11.1.7), a physiologically derived enzyme from neutrophils (white blood cells), generates potent ROS including HOCl (from NaCl and H_2O_2), which is thought to contribute to the degradation of implantable polymeric materials.[36] hMPO is a 150 kDa dimeric protein with active heme cofactors, analogous to CPO, and is shown as the tertiary structure in Figure 6A. Unlike CPO, only a single dose of 500 μM H_2O_2 was subjected to hMPO (5 U/mL) in an effort to conserve enzymatic activity. As illustrated in Figure 6B, a single dose generates a similar concentration of ROS to CPO in the same 30 min time regime, albeit at a lesser enzyme concentration. It is important to note, however, that hMPO's optimum activity is at pH 4.5. In performing experiments at pH 6.02, we likely see an increased activity of hMPO relative to CPO as a result of this pH effect. Thus, for turbidity measurements, a 2 mL aliquot of PPS-encapsulated Nile red particles was suspended in 100 mM phosphate buffer (pH 6.02) with 5 U/mL hMPO and 200 mM NaCl and subjected to a single 500 μM dose of H_2O_2. As performed previously, a stable baseline was observed for the first five minutes prior to the addition of H_2O_2. Indicated in Figure 6C, a single dose of H_2O_2 stimulates a 10% increase in particle turbidity over the course of 30 minutes. In comparison, a single dose of buffer does not significantly alter the transmittance observed for PPS nanoparticles (black trace). If such data are truly analogous to CPO, a 10 percent change in transmittance

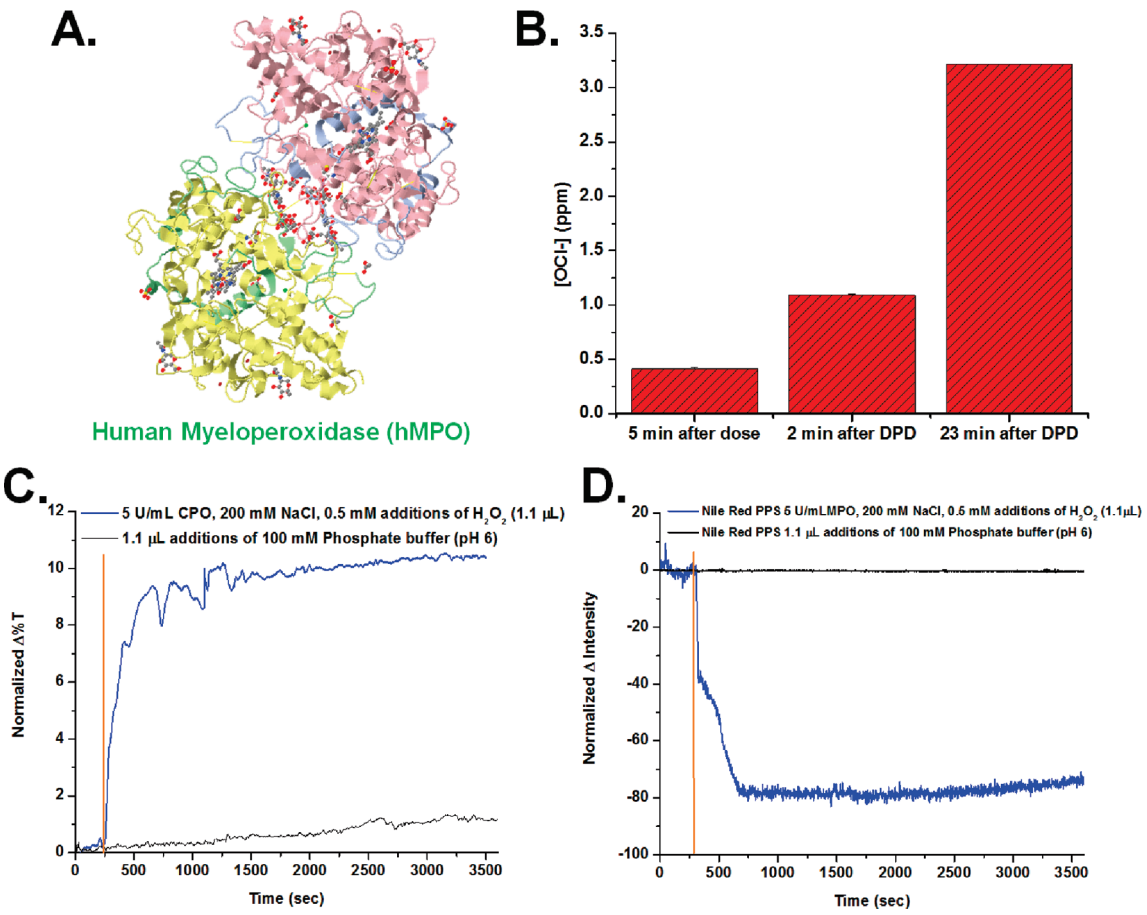

Figure 6. (A) Tertiary structure of human myeloperoxidase. (B) A single dose of 500 μM H_2O_2 generated 3.25 ppm of ROS species over 30 min. (C) Normalized turbidity measurements of PPS particles oxidized by hMPO-generated ROS. (D) Normalized spectrofluorimetric measurements of Nile red release by hMPO-mediated PPS particle swelling.

should translate into the release of Nile red dye as observed by spectrofluorimetric analysis. Indeed, when the same conditions were analyzed by spectrofluorimetry, an 80% decrease in emission intensity was observed upon exposure to a single dose of 500 μM H_2O_2, as indicated in Figure 6D. Such results correspond well with those previously obtained with chemical oxidation of PPS-encapsulated Nile red nanoparticles by NaOCl and CPO-mediated particle swelling.

CONCLUSIONS

To conclude, we have illustrated the synthesis of poly(propylene sulfide) nanoparticles and their subsequent encapsulation of hydrophobic molecular cargo. Reichardt's and Nile red dyes were encapsulated in PPS nanoparticles, and their analyte-specific release was triggered both chemically and enzymatically by ROS generation. Of important note, we have demonstrated that physiologically relevant enzymes such as hMPO can drive the release of encapsulated molecular cargo. These results allude to the ability of PPS nanoparticles, potentially capable of encapsulating a variety of hydrophobic cargo including antibiotics and antimicrobials, to deliver and release relevant species in a controlled environment. Such a unique feature may have future applications in drug delivery and inflammation remediation, pending successful cellular-based studies.

MATERIALS AND METHODS

Synthesis of Poly(propylene sulfide) Nanoparticles. Nanoparticles were synthesized by degassing 90 mL of deionized water with N_2 gas under 200 rpm stirring for approximately 1 h. Following, 1.0 g of Pluronic F-127 surfactant was added to the stirring reactor, which was sealed and degassed for an additional 1 h. Propylene sulfide (final concentration: 0.25 M) was then added to the reactor at 1000 rpm stirring at a volume of 2.0 mL. This was allowed to incubate for 10–15 min. Concurrently, 0.24 g of pentaerythritol tetrathioester was deprotected by 800 μL of 0.5 M sodium formate (MeOH) by stirring for 10 min and injecting this entire volume into the stirring reactor. After incubation for 15 min, the reaction was initiated by the addition of 10 mL of 100 mM borate buffer (pH 9.0). Polymerization was allowed to continue for 24 h under a N_2 atmosphere and at 1000 rpm stirring. Following the polymerization, free thiolates were capped by the

addition of 600 μL of iodoacetamide (IDA) or allowing disulfide linkages to form under air oxidation.

For the encapsulation of hydrophobic dyes, an analogous protocol was utilized with the following exception: Reichardt's dye or Nile red dye was added to the reactor prior to the addition of propylene sulfide. Approximately 10 mg of the respective dye was added and allowed to solubilize for 30 min prior to the addition of propylene sulfide.

***N,N*-Diethyl-*p*-phenylenediamine Sulfate End Point Assay.** A 5% (v/v) DPD stock solution (4.21 mM DPD and 0.54 mM ethylenediaminetetraacetic acid (EDTA) solution (aq)) and a 5% (v/v) [0.5 M] sodium−potassium phosphate buffer were added to aqueous samples and immediately assayed for absorbance at λ 540 nm.

Characterization. Low-resolution TEM images were obtained with a Philips/FEI Morgagni microscope. The electron beam accelerating voltage of the TEM was held at 80.0 keV for all imaging. All samples were prepared by suspending PPS nanoparticles in DI water, drop-casting on a carbon-coated TEM grid (Electron Microscopy Sciences), and allowing water to completely evaporate.

Absorbance spectroscopy was performed on a Perkin-Elmer Lambda 25. Turbidity of PPS nanoparticles was measured at 600 nm as a function of time. Samples were serially diluted until an average percent transmittance of 50% was obtained. A working volume of 2 mL was used for all studies in 100 mM phosphate buffer (pH 6.02). To account for deviation in particle samples, all data were normalized to the first five minutes of sampling, prior to addition of activating species.

Fluorescence spectroscopy was performed on a Jasco FP 6500 spectrofluorimeter. Spectral mapping was performed by scanning excitation wavelengths from 400 to 490 nm and emission wavelengths from 500 to 700 nm. For all experiments, an excitation and emission bandwidth of 5 nm was used, with a 0.2 s sampling rate.

Acknowledgment. We gratefully acknowledge funding for this work provided by the Army Research Office under grant # W911NF-09-C-0156. The authors also acknowledge Dr. Jason Berberich and Jessica Sinclair for their helpful discussion with enzymatic studies, and Dr. Justin Bohn for his discussion with emulsion polymerizations.

Supporting Information Available: A detailed description can be found of dynamic light scattering data, internal volume calculations, Reichardt's dye oxidation controls, dye encapsulation controls, spectral mapping, dye loading quantification, efficiency of dye encapsulation, H_2O_2 effects on PPS nanoparticles, calibration plots for DPD assays, and enzymatic optimization conditions. This material is available free of charge *via* the Internet at http://pubs.acs.org.

REFERENCES AND NOTES

1. Zhao, M.; Beauregard, D. A.; Loizou, L.; Davletov, B.; Brindle, K. M. Non-Invasive Detection of Apoptosis Using Magnetic Resonance Imaging and a Targeted Contrast Agent. *Nat. Med.* **2001**, *7*, 1241–1244.
2. Mathiowitz, E.; Jacob, J. S.; Jong, Y. S.; Carino, G. P.; Chickering, D. E.; Chaturvedi, P.; Santos, C. A.; Vijayaraghavan, K.; Montgomery, S.; Bassett, M.; *et al.* Biologically Erodable Microspheres As Potential Oral Drug Delivery Systems. *Nature* **1997**, *386*, 410–414.
3. Sosnik, A.; Carcabosa, A. M.; Glisoni, R. J.; Moretton, M. A.; Chiappetta, D. A. New Old Challenges in Tuberculosis: Potentially Effective Nanotechnologies in Drug Delivery. *Adv. Drug Delivery Rev.* **2010**, *62*, 547–559.
4. Sukhorukov, G. B.; Rogach, A. L.; Garstka, M.; Springer, S.; Parak, W. J.; Muñoz-Javier, A.; Kreft, O.; Skirtach, A. G.; Susha, A. S.; Ramaye, Y.; *et al.* Multifunctionalized Polymer Microcapsules: Novel Tools for Biological and Pharmacological Applications. *Small* **2007**, *3*, 944–955.
5. Kim, E.; Kim, D.; Jung, H.; Lee, J.; Paul, S.; Selvapalam, N.; Yang, Y.; Lim, N.; Park, C. G.; Kim, K. Facile, Template-Free Synthesis of Stimuli-Responsive Polymer Nanocapsules for Targeted Drug Delivery. *Angew. Chem., Int. Ed.* **2010**, *49*, 4405–4408.
6. Gaponik, G.; Radtchenko, I. L.; Gerstenberger, M. R.; Fedutik, Y. A.; Sukhorukov, G. B.; Rogach, A. L. Labeling of Biocompatible Polymer Microcapsules with Near-Infrared Emitting Nanocrystals. *Nano Lett.* **2003**, *3*, 369–372.
7. Shchunkin, D. G.; Radtchenko, I. L.; Sukhorukov, G. B. Micron-Scale Hollow Polyelectrolyte Capsules with Nanosized Magnetic Fe_3O_4 Inside. *Mater. Lett.* **2003**, *57*, 1743–1747.
8. Ma, Y.; Dong, W. − F.; Hempenius, M. A.; Möhwald, H.; Vancso, G. J. Redox-Controlled Molecular Permeability of Composite-Wall Microcapsules. *Nat. Mater.* **2006**, *5*, 724–729.
9. Broaders, K. E.; Pastine, S. J.; Grandhe, S.; Fréchet, J. M. J. Acid-Degradable Solid-Walled Microcapsules for pH-Responsive Burst-Release Drug Delivery. *J. Am. Chem. Soc.* **2011**, *47*, 665–667.
10. Xiong, X. Y.; Tam, K. C.; Gan, L. H. Release Kinetics of Hydrophobic and Hydrophilic Model Drugs from Pluronic F127/poly(Lactic Acid) Nanoparticles. *J. Controlled Release* **2005**, *103*, 73–82.
11. Sullivan, C. O.; Birkinshaw, C. *In vitro* Degradation of Insulin-Loaded poly(n-Butylcyanoacrylate) Nanoparticles. *Biomaterials* **2004**, *25*, 4375–4382.
12. Kim, J.-H.; Kim, Y.-S.; Park, K.; Kang, E.; Lee, S.; Nam, H. Y.; Kim, K.; Park, J. H.; Chi, D. Y.; Park, R.-W.; *et al.* Self-Assembled Glycol Chitosan Nanoparticles for the Sustained and Prolonged Delivery of Antiangiogenic Small Peptide Drugs in Cancer Therapy. *Biomaterials* **2008**, *29*, 1920–1930.
13. Sarmento, B.; Ribeiro, A.; Veiga, F.; Sampaio, P.; Neufeld, R.; Ferreira, D. Alginate/Chitosan Nanoparticles are Effective for Oral Insulin Delivery. *Pharm. Res.* **2007**, *24*, 2198–2206.
14. Ferrero-Miliani, L.; Nielsen, O. H.; Andersen, P. S.; Girardin, S. E. Chronic Inflammation: Importance of NOD2 and NAL3 in Interleukin-1β Generation. *Clin. Exp. Immunol.* **2007**, *147*, 227–235.
15. Broaders, K. E.; Grandhe, S.; Fréchet, J. M. J. A Biocompatible Oxidation-Triggered Carrier Polymer with Potential in Therapeutics. *J. Am. Chem. Soc.* **2011**, *133*, 756–758.
16. Han, P.; Ma, N.; Ren, H.; Xu, H.; Li, Z.; Wang, Z.; Zhang, X. Oxidation-Responsive Micelles Based on a Selenium-Containing Polymeric Superamphiphile. *Langmuir* **2010**, *26*, 14414–14418.
17. Rehor, A.; Tirelli, N.; Hubbell, J. A. A New Living Emulsion Polymerization Mechanism: Episulfide Anionic Polymerization. *Macromolecules* **2002**, *35*, 8688–8693.
18. Rehor, A.; Hubbell, J. A.; Tirelli, N. Oxidation-Sensitive Polymeric Nanoparticles. *Langmuir* **2005**, *21*, 411–417.
19. Rehor, A.; Schmoekel; Tirelli, N.; Hubbell, J. A. Functionalization of Polysulfide Nanoparticles and Their Performance As Circulating Carriers. *Biomaterials* **2008**, *29*, 1958–1966.
20. Rothenfluh, D. A.; Bermudez, H.; O'Neil, C. P.; Hubbell, J. A. Biofunctional Polymer Nanoparticles for *Intra*-Articular Targeting and Retention in Cartilage. *Nat. Mater.* **2008**, *7*, 248–254.
21. White, G. C. *Handbook of Chlorination*, 2nd ed.; Van Nostrand Reinhold: New York, NY, 1986; pp 150−213.
22. Napoli, A.; Valentini, M.; Tirelli, N.; Müller, M.; Hubbell, J. A. Oxidation-Responsive Polymeric Vesicles. *Nat. Mater.* **2004**, *3*, 183–189.
23. Reichardt, C. Solvatochromic Dyes As Solvent Polarity Indicators. *Chem. Rev.* **1994**, *94*, 2319–2358.
24. Sackett, D. L.; Wolff, J. Nile Red As a Polarity-Sensitive Fluorescent Probe of Hydrophobic Protein Surfaces. *Anal. Biochem.* **1987**, *167*, 228–234.
25. Greenspan, P.; Mayer, E. P.; Fowler, S. D. Nile Red: a Selective Fluorescent Stain for Intracellular Lipid Droplets. *J. Cell. Biol.* **1985**, *100*, 965–973.
26. Lampe, J. N.; Fernandez, C.; Nath, A.; Atkins, W. M. Nile Red is a Fluorescent Allosteric Substrate of Cytochrome P450 3A4. *Biochemistry* **2008**, *47*, 509–516.
27. Schreiner, K. M.; Filley, T. R.; Blanchette, R. A.; Bowen, B. B.; Bolskar, R. D.; Hockaday, W. C.; Masiello, C. A.; Raebiger, J. W. White-Rot Basidiomycete-Mediated Decomposition of C_{60} Fullerol. *Environ. Sci. Technol.* **2009**, *43*, 3162–3168.
28. Allen, B. L.; Kichambare, P. D.; Gou, P.; Vlasova, I. I.; Kapralov, A. A.; Konduru, N.; Kagan, V. E.; Star, A. Biodegradation of

Single-Walled Carbon Nanotubes through Enzymatic Catalysis. *Nano Lett.* **2008**, *8*, 3899–3903.
29. Kagan, V. E.; Konduru, N. V.; Feng, W.; Allen, B. L.; Conroy, J.; Volkov, Y.; Vlasova, I. I.; Belikova, N. A.; Yanamala, N.; Kapralov, A.; *et al*. Carbon Nanotubes Degraded by Neutrophil Myeloperoxidase Induce Less Pulmonary Inflammation. *Nat. Nanotechnol.* **2010**, *5*, 354–359.
30. Winterbourn, C. C. Reconciling the Chemistry and Biology of Reactive Oxygen Species. *Nat. Chem. Biol.* **2008**, *4*, 278–286.
31. Amitai, G.; Adani, R.; Hershkovitz, M.; Bel, P.; Rabinovitz, I.; Meshulam, H. Degradation of VX and Sulfur Mustard by Enzymatic Haloperoxidation. *J. Appl. Toxicol.* **2003**, *23*, 225–233.
32. Libby, R. D.; Shedd, A. L.; Phipps, A. K.; Beachy, T. M.; Gerstberger, S. M. Defining the Involvement of HOCl or Cl_2 As Enzyme-Generated Intermediates in Chloroperoxidase-Catalyzed Reactions. *J. Biol. Chem.* **1992**, *267*, 1769–1775.
33. Libby, R. D.; Beachy, T. M.; Phipps, A. K. Quantitating Direct Chlorine Transfer from Enzyme to Substrate in Chloroperoxidase-Catalyzed Reactions. *J. Biol. Chem.* **1996**, *271*, 21820–21827.
34. Grinstead, R. R. The Oxidation of Ascorbic Acid by Hydrogen Peroxide. Catalysis by Ethylenediaminetetraacetato-Iron(III). *J. Am. Chem. Soc.* **1960**, *82*, 3464–3471.
35. Moore, H. E.; Garmendia, M. J.; Cooper, W. J. Kinetics of Monochloramine Oxidation of N,N-Diethyl-p-Phenylenediamine. *Environ. Sci. Technol.* **1984**, *18*, 348–353.
36. Sutherland, K.; Mahoney, J. R.; Coury, A. J., II; Eaton, J. W. Degradation of Biomaterials by Phagocyte-Derived Oxidants. *J. Clin. Invest.* **1993**, *92*, 2360–2367.